Efficient hydrogen production using Cu-based catalysts prepared *via* homogeneous precipitation

Yu-Kai Lin,[a] Yi-Han Su,[b] Yun-Hsin Huang,[b] Chia-Jung Hsu,[b] Yu-Kuei Hsu,[c] Yan-Gu Lin,[d] Ko-Hsiung Huang,[b] San-Yuan Chen,[d] Kuei-Hsien Chen*[ac] and Li-Chyong Chen*[a]

Received 22nd June 2009, Accepted 30th September 2009
First published as an Advance Article on the web 29th October 2009
DOI: 10.1039/b912253b

We report here preparation of multi-composition $Cu/ZnO/Al_2O_3$ (CZA) catalyst by homogeneous precipitation (HP) method using urea treatment. Compared to the conventional co-precipitation (CP) method, the HP method used here improves the uniformity of metal mixing through homogeneous generation of hydroxide ions as a result of hydrolysis of urea in the solution. In this study, optimization of the conditions to prepare CZA catalyst was achieved by adjusting the urea concentration, amount of water, reaction temperature and reaction time; to control the pH value. The HP-derived CZA particles exhibited a characteristic flower-like morphology with a higher surface area, typically 78.5 m^2/g as measured by the BET analysis, as compared to the CP-derived CZA catalysts. Induction coupled plasma and energy dispersive spectroscopy mapping results further confirmed the homogeneity of HP-CZA components and highly uniform dispersion of the active metal. Significantly lowering and a narrower range of the reduction temperature for HP-CZA is observed. An improved performance in methanol reforming reaction, in terms of methanol conversion, yield of hydrogen production, and higher carbon dioxide selectivity, has been achieved. Furthermore, the concentration of carbon monoxide can be further reduced by employing CeO_2 and ZrO_2 to modify the support, which also results in reduced reduction temperature and improved performance. Among the modified catalysts, HP-CZCZ catalyst showed the highest methanol conversion and rate of hydrogen production, simultaneously with reduced concentration of CO. Moreover, only 20 mg of catalyst loading yielded 98% methanol conversion rate under more than 8500 h^{-1} GHSV. In future, not only can this method be used to synthesize other multi-composition materials with high homogeneity, but also our approach presents opportunity for production of a highly active catalyst for efficient generation of hydrogen for fuel cell applications.

Introduction

Due to the ever increasing demand for energy, an effective alternative energy generation capability is essential to replace the dwindling supply of petroleum. In comparison to the several novel energy generation techniques, hydrogen is one of the most environmentally friendly sources. However, the challenges associated with supply and storage of hydrogen are enormous obstacles for its industrial scale application. In this regard, the reforming reaction of methanol is considered to be an attractive option for hydrogen generation, because of the ease of handling and possibility of hydrogen synthesis from various feedstocks[1] by this method. Moreover, methanol also happens to be the best source for hydrogen generation among the high energy density liquid fuels, due to its high H/C ratio, and consequently a lower propensity for soot formation than other hydrocarbons; relatively low boiling point and easy storage and handling requirements.[2]

Extraction of hydrogen from methanol can be performed by three different catalytic processes: *viz.* decomposition (MD: Eq. (1)), steam reforming (SRM: Eq. (2)), and partial oxidation (POM: Eq. (3)).[3–10]

$$CH_3OH \rightarrow CO + 2H_2 \quad \Delta H^\circ = +90.5 \text{ kJ/mol} \qquad (1)$$

$$CH_3OH + H_2O \rightarrow CO_2 + 3H_2 \quad \Delta H^\circ = +49.4 \text{ kJ/mol} \qquad (2)$$

$$CH_3OH + 1/2O_2 \rightarrow CO_2 + 2H_2 \quad \Delta H^\circ = -192.2 \text{ kJ/mol} \qquad (3)$$

Besides these three reactions, oxidative steam reforming of methanol (OSRM), which combines the endothermic steam reforming reaction with the exothermic partial oxidation reactions (Eq. (4))[11–15] can also be used. By proper optimization of reaction parameters and system design, favorable hydrogen production rate can be achieved while eliminating the requirement of any external heat for the reaction. Therefore, OSRM is also called the autothermal reaction. In addition, SRM can be regarded as MD plus a water gas shift (WGS: Eq. (5)) pathway, which is an important reaction for CO reduction.

[a]*Center for Condensed Matter Sciences, National Taiwan University, Taipei, Taiwan. E-mail: chenkh@pub.iams.sinica.edu.tw; chenlc@ntu.edu.tw*
[b]*Taipei First Girls High School, Taipei, Taiwan*
[c]*Institute of Atomic and Molecular Sciences, Academia Sinica, Taipei, Taiwan*
[d]*Department of Materials Science and Engineering, National Chiao Tung University, Hsinchu, Taiwan*

$$CH_3OH + aO_2 + bH_2O \rightarrow CO_2 + (4a+3b)H_2 (a,b \text{ are varied}) \quad \Delta H^\circ = (-96.1a + 49.4b) kJ/mol \tag{4}$$

$$CO + H_2O \rightarrow CO_2 + H_2 \quad \Delta H^\circ = -41.1 \text{ kJ/mol} \tag{5}$$

For methanol reforming reaction, Cu-based catalysts such as $Cu/ZnO/Al_2O_3$ (CZA) system are used most extensively, due to their low cost, high selectivity and high catalytic activity.[13–16] The dispersion of active Cu metal and its surface area play a crucial role in determining the catalytic activity and stability of these catalysts. A large number of researchers have employed a co-precipitation (CP) method to prepare Cu-based catalysts.[9–12,16–20] However, this method suffers from a gradient in concentration of hydroxide ions during the precipitation process, which results in the poor mixing and growth of precipitates.[8,14,21] In order to improve the uniformity of precipitates, a homogeneous precipitation (HP) method was employed in this research.[8,13,21,22] Hydrolysis of urea was used to generate hydroxide ions homogeneously in the solution without a gradient in concentration. In order to obtain the optimum precipitation conditions, the effects of four major parameters—*viz.* urea concentration, amount of water, reaction temperature and reaction time—were studied. For the CZA catalyst system, the correlation between the morphology and crystal structures of the precipitate precursors and its catalytic performance are known to be different for different methods of synthesis. A CP-derived CZA catalyst was, hence, prepared for comparison. In addition, the possibilities of applying HP method towards synthesis of other multi-compositional compounds, as well as towards improvement in the catalytic performance of CZA catalyst are also discussed.

Experimental

Preparation of the catalysts

The $Cu/ZnO/Al_2O_3$ (CZA) catalysts as well as the modified catalysts with various compositions were prepared *via* homogeneous precipitation (HP) method. Aqueous solutions of metal nitrates and urea were mixed at a given concentration at room temperature, followed by heating at appropriate temperature for several hours. The pH value of the reacted solution was controlled between 7 and 8, in order to ascertain that all metal ions were precipitated. During the heating progress, urea was hydrolyzed, generating hydroxide ions homogeneously in the solution (Eq. (6)).

$$CO(NH_2)_2 + H_2O \rightarrow 2NH_4^+ + HCO_3^- + OH^- \tag{6}$$

The hydroxide ions act as precipitants for the metal species. It is, hence, anticipated that homogeneous precipitation method would afford catalysts with high homogeneity as compared to the conventional co-precipitation (CP) method. Thus, the concentration gradient of hydroxide ions may be reduced. The precipitates were then filtered, washed with de-ionized water and dried at 90 °C overnight. The CZA precursors were calcined at 300 °C for 3h in air. The obtained powders were then pressed, crushed and sieved using a 30 to 40 mesh. In addition, the co-precipitation method derived CZA catalyst was also prepared as a comparison. In this method, the starting materials, metal nitrates, were dissolved in the water to form aqueous solution with the same metal ion ratio and solution concentration as those in HP method. Na_2CO_3 solution (1M) was prepared as base source and added drop-wisely to the previous solution with vigorous stirring at 60 °C while the pH value was controlled to 8, and then aged for 2 hours. The catalyst was thus obtained by the same following filtration, drying, and calcination steps as those in HP method.

Characteristics measurement and activity test

The catalysts, prepared as described above, were characterized by X-ray powder diffraction (Bruker D8 Advance). The diffraction patterns were identified by comparing with those in the JCPDS (Joint Committee of Powder Diffraction Standards) database. The microstructures of catalysts were determined by using JEOL 6700 field-emission scanning electron microscope (SEM).

Chemical compositions of the catalysts were determined by inductively coupled plasma optical emission spectrometry (ICP-OES). The samples were dissolved in HNO_3 acid for the ICP-OES measurements. The metal compositions, as obtained by the ICP-OES measurements, closely matched with the stoichiometric values used for catalyst preparation.

The specific surface areas of the catalysts were calculated from the N_2 adsorption isotherms by using the BET method. These measurements were carried out on a Micrometry Tristar equipment. The samples were pretreated under vacuum at 200 °C for 1h before the measurements.

The specific surface area of copper and copper dispersion of catalysts were determined by the method of reaction with N_2O ($2Cu_{(s)} + N_2O_{(g)} \rightarrow Cu_2O_{(s)} + N_{2(g)}$)[23] followed by temperature programmed reduction (TPR) in a semiautomatic Micromeritics TPD/TPR 2920 apparatus fitted with a thermal conductivity detector (TCD) and interfaced to a microcomputer. The sample of 20 mg was pre-reduced in a stream of 10% H_2/Ar flow (50 ml/min) by raising the temperature to 350 °C at a rate of 10 °C/min before chemisorption. Then, N_2O oxidation was carried out by feeding 10% N_2O/He at 60 °C for 1 hour. Finally, H_2-TPR was treated again in a 10% H_2/Ar mixture to 350 °C. The nitrous oxide was assumed to react selectively with the reduced surface copper atom, without oxidation of bulk copper. Cu surface area and Cu dispersion were calculated assuming the stoichiometry O/Cu = 0.5 and the surface density of 1.46×10^{19} Cu-atoms/m^2.[23]

Catalytic reactions and analyses of the products

Measurements of the catalytic activity were performed by carrying out oxidative steam reforming of methanol (OSRM) reaction using a fixed-bed system at atmospheric pressure. A glass tube with an inner diameter of 1/4 inches was used as a reactor. Typically, 20 mg sieved catalysts were packed in the middle of the glass tube by two pieces of quartz wool on both sides. A thermal couple was placed at the center of the catalyst bed. Prior to the methanol reforming reaction and also between different runs, the catalysts were flushed with N_2 followed by reduction at 350 °C with 10% H_2/N_2 mixture (50 ml/min) for 1h.

After purging with N_2 to remove any remaining H_2, the reactants were introduced into the reactor with the molar ratio $O_2/CH_3OH = 0.3$ and $H_2O/CH_3OH = 1.25$, respectively. N_2 was used both as the carrier gas as well as internal standard to calculate the conversion of methanol, selectivity of CO_2/CO, and the H_2 production rate. GHSV was kept constant at around 8900 h^{-1}, and the reaction temperature was also kept constant at 250 °C.

The products were analyzed by three on-line gas chromatographs (GC) in series. The first GC consisted of packed porapak Q column, He carrier gas, and TCD, was used to analyze N_2, CH_3OH, CO_2, and H_2O. The second GC consisted of a packed molecular sieve 13X column, He carrier gas, and TCD, was used to analyze CO, CH_4 and other hydrocarbons. Between these two GCs, a cooling system was equipped to condense CH_3OH and H_2O from the gas mixture. H_2 and N_2 were also quantified by the third GC consisting of a packed molecular sieve 13X column with Ar carrier gas and TCD. Each injection through the GCs was 1 c.c., controlled by three automatic valves at a given time interval. The temperatures of pipe lines before the cooling system and the three valves were maintained between 110 °C and 130 °C in order to prevent any condensation of water.

Results and discussion

pH value measurement and precipitation observation

Since urea and water are reactants for the urea hydrolysis reaction, the concentration ratio of urea to metal ions as well as to total solution are important parameters that have significant effect on the precipitation process. In this study, the influence of the urea concentrations was studied while the concentration of metal ions was kept constant. In addition, since water has a pH value of 7, higher than that of the initial solutions (3.4–3.9), and also acts as reactant in the urea hydrolysis reaction, it is expected that the pH values can be adjusted by addition of water in varying quantities. Water is also a desirable material to adjust the pH values of the solution due to its ease of handling.

Fig. 1 shows the photographs of the products after the urea hydrolysis reaction. As can be seen in Fig. 1 (a), significant increase in the pH value was observed for both, increase in urea concentration as well as amount of water. However, the target pH value of 7 to 8 was obtained only for 4M urea solution or when 3 times water was added to the 3M urea solution. Among these four conditions, the 4M urea solutions with 1/2 dilution ratio and without dilution are light blue, while the other solutions appear colorless. The precursors prepared with 3M urea and 1/4 dilution ratio was considered to be the better condition. First, among the 3M and 4M solutions with favorable pH values, blue colors were observed only for the 4M solutions. This indicates a decrease in the amount of copper in the precipitates, owing to the formation of copper complexes in the solution. Second, the ICP results further prove that the fraction of metal in the precipitates obtained under 3M urea condition is close to the initial value. Third, from the economic point of view, 3M condition consumes less urea than 4M. Thus, the precipitation condition of 3M urea was used in the subsequent experiments.

Fig. 1 (b) shows the photographs of the products after the reaction at various temperatures and for various times. These experiments to obtain the kinetic parameters were performed by keeping the amount of water and urea concentration constant. The pH values of solutions obviously increase with both longer reaction time as well as higher reaction temperature. In addition, it can also be observed that the pH value is more sensitive to the reaction temperature as compared to the reaction time. When the pH values were higher than 8, formation of deep blue solutions were observed and the color of precipitates was darker as well, both of which are undesirable for the precipitation. The blue color results from the formation of Cu complexes in the solution, while the dark particles derive from the formation of CuO. Once CuO is formed during the precipitation process, it deteriorates the hydrotalcite-like structure of the precipitates and influences the morphology of the products.[24,25] It has also been suggested that reactions performed at 100 °C are inappropriate for hydrolysis process due to the violent boiling phenomena within the solutions, and different equilibrium ratio between liquid phase water and steam compared with low temperature reaction. Thus, heating at 95 °C for two hours was selected to be a better synthesis condition.

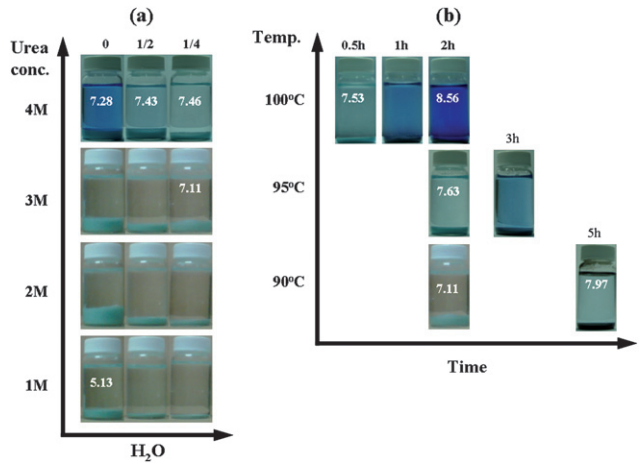

Fig. 1 Observation of precipitation results controlled by (a) urea concentration and water amount, and (b) reaction temperature and duration time.

Structure and morphology analysis of the CZA catalysts

X-ray diffraction (XRD) patterns of the precursors synthesized at different temperatures and reaction times are shown in Fig. 2. Strong diffraction peaks related to azurite structure $(Cu_3(CO_3)_2(OH)_2$; JCPDS file 11-0682) are apparent in the 1M urea sample, Fig. 2 (a), indicating this being a highly preferred orientation. From the scanning electron microscope (SEM) images as illustrated in Fig.3 (a), this sample can also be seen to exhibit a plate-like morphology, which further confirms the results of XRD. Moreover, in Fig. 1 (a), the pH value of the 1M urea sample without dilution was 5.13. It has been shown that at this pH value, the precipitates consist primarily of Cu compounds, and not many Zn ions are precipitated.[25] ICP results also confirmed the composition of these precipitates to be consisting of a large percentage of Cu. After being calcined at 300 °C, only the CuO (JCPDS file 45-0937) diffraction lines could be seen in the XRD pattern. With an increase in urea concentration and water dilution, as shown in Fig. 2 (b), the samples prepared at

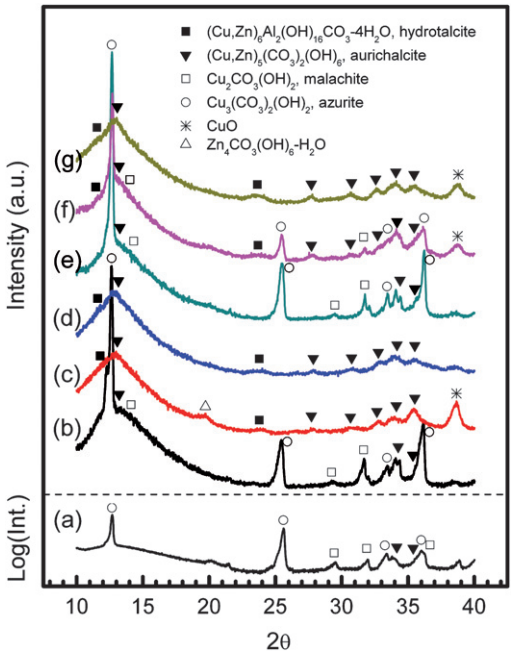

Fig. 2 XRD patterns of precipitates under different reaction conditions (a) urea = 1M 90 °C for 2h, and urea = 3M with 1/4 dilution ratio (b) 90 °C for 2h, (c) 90 °C for 5h, (d) 95 °C for 2h, (e) 100 °C for 0.5h, (f) 100 °C for 1h, (g) 100 °C for 2h.

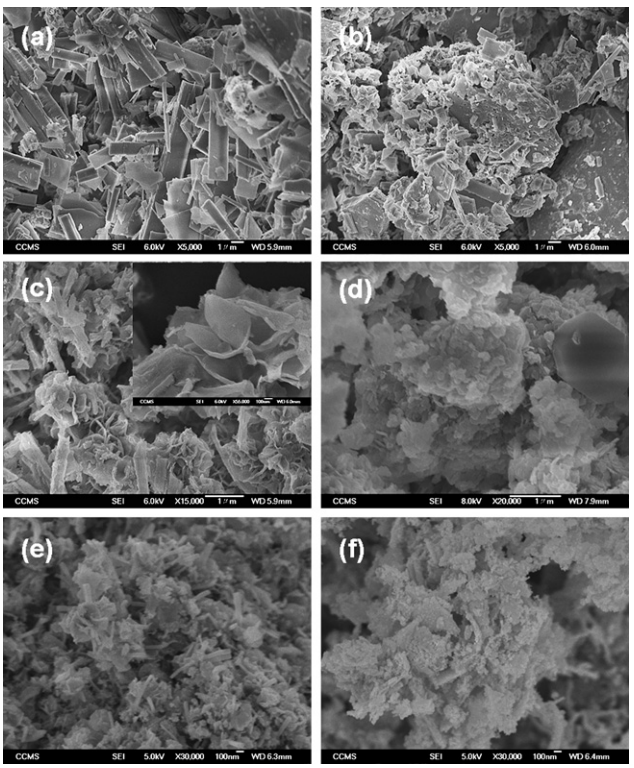

Fig. 3 SEM images of (a) urea = 1M w/o dilution, (b) urea = 3M w/o dilution, (c) urea = 3M with 1/4 dilute ratio 95 °C for 2h (HP-CZA precursor), (d) CP-CZA precursor, (e) reduced HP-CZA catalyst, and (f) reduced CP-CZA catalyst.

3M urea with 1/4 dilution ratio exhibit relatively weak azurite peaks while clearly displaying aurichalcite ($(Cu,Zn)_5(CO_3)_2(OH)_6$; JCPDS file 17-0743) and hydrotalcite ($(Cu,Zn)_6Al_2CO_3(OH)_{16}$; JCPDS file 37-0629) peaks.

The crystal structure corresponding to aurichalcite (Cu/Zn ratio is 0.67) phase crystallizes in the monoclinic space group $P2_1/m$ (C^2_{2h}).[26] Four different Me^{2+} sites in this lattice are Me(1) (C_s site symmetry) and Me(2) (C_1 site symmetry), which are tetragonally distorted octahedral sites; while Me(3) and Me(4) (both are C_s site symmetry) have tetrahedral and trigonal bipyramidal coordination, respectively. Me(1), Me(2), and Me(4) sites are occupied by Cu and Zn with equal probability, while Me(3) is entirely occupied by Zn. Similar to aurichalcite, hydrotalcite is also a layered-structure compound. In its molecular structure matrix, all of the metal ions are located in the center of the hydroxide octahedral structures, and CO_3^{2-} groups are located between the hydroxide octahedral layers.[27] This implies that the metal ions are well separated by the hydroxide ions and highly dispersed in the aurichalcite or hydrotalcite structure matrix. In addition, it has been shown that when these hydrotalcite-like structures are heated to 450 °C in air ambiance, even the crystalline phases convert into metal oxides, while the local bonding environment and electronic state of Cu ions remain unchanged.[28] It has also been reported that the intensity of the XRD peaks related to aurichalcite phase has a positive correlation with the activity of the Cu-based catalysts.[21] Therefore, the precipitates that consist of such structures are believed to be appropriate precursors for the catalyst applications.

A comparison between the diffraction lines in Fig. 2 (b), (d), and (g) shows that azurite and malachite ($Cu_2CO_3(OH)_2$; JCPDS file 41-1390) phases disappear when the reaction temperature increases from 90 °C to 95 °C, and the formed alternative phases are aurichalcite and hydrotalcite. The molecular structures of azurite and malachite are based on Cu ions, but aurichalcite and hydrotalcite structure are formed by Cu, Zn, and/or Al ions. In addition, the pH values of the corresponding two samples in Fig.1 (b) are 7.11 and 7.63. Thus, this indicates that most of Zn and Al ions are precipitated between these two pH values, and cause change in the structures of the precipitates. Further increasing the reaction temperature to 100 °C is not beneficial for precipitation since some fraction of precipitated Cu compounds can be seen to oxidize to form CuO, in Fig. 2 (g). Besides, the deep blue color of the corresponding solution indicates that a large fraction of the remaining Cu ions are depleted by the ammonia to form the Cu complexes, consequently making the metal composition of precipitates to deviate from the initial preparation. Thus, 95 °C is seen to be an optimum temperature for preparation of this catalyst.

At 100 °C reaction temperature, as illustrated in Fig. 2 (e), (f), and (g), with increase in reaction time, the azurite and malachite phases gradually shift to aurichalcite and hydrotalcite phases as well as reduce the preference towards orientation of the azurite phase. However, an obvious color change of the solutions indicates a rapid reaction between Cu ions and ammonia at 100 °C. Also, CuO phase was detected for the 1h and 2h samples. This accelerated reaction could mainly result from the enhanced reaction kinetics at high temperature. By increasing the reaction time from 2h to 5h at 90 °C, the XRD pattern was found to be similar to the sample prepared at 100 °C for 2h, as shown in

Fig. 2 (c). An obvious CuO peak can be seen, indicating that though hydrotalcite-like structures can be obtained by increasing the reaction time at relative low temperature (90 °C), the oxidation of precipitates also become more serious.

In order to obtain the optimum preparation conditions, the effects of urea concentration, amount of water, reaction temperature and the time of urea hydrolysis reaction were studied. Among these four parameters, reaction temperature was found to play the most influential role in the current precipitation process. As shown in Fig. 1 (b) and Fig. 2, under the condition of 3M urea with 1/4 dilution ratio, the pH values increased from 7.11 to 8.56 for increase in the reaction temperature by only 10 °C. In addition, variations in temperature were also found to significantly influence the colors of solution and precipitates as well as the structure of precipitates, especially at higher temperatures. 100 °C was not found to be an appropriate temperature for the urea hydrolysis reaction because of the associated promotion of side reactions and increased oxidation for Cu compounds during the precipitation process. Besides, boiling of the solution during reaction would not only change the equilibrium ratio of liquid to vapor, but also the concentration of solution, affecting the composition of final product.

Since various combinations of the reaction conditions are possible for the catalyst preparation, four parameters were used to select the optimum conditions. First, the pH value was monitored and controlled between 7 and 8. Second, the color of the solution and precipitates was observed to help judge the composition of the product. Third, ICP analyses were used to confirm the composition of the product. Fourth, XRD patterns were studied to characterize the crystallinity and detect existence of various crystalline phases in the product. Only when the product conformed to the expectations from these four parameters, then the catalyst was chosen to proceed to the catalytic activity test. Among all the experimental conditions, 3M urea with 1/4 dilution ratio and temperature of 95 °C for 2 h was selected as the preferable condition and named as HP-CZA, based on its appropriate pH value, its colorless solution, close matching of its chemical composition with preparation condition, and the hydrotalcite-like structure of precipitates.

In order to compare the effects of precipitation method on the performance of the catalyst, a co-precipitation method derived sample was also prepared and named as CP-CZA. The chemical composition of CP-CZA was the same as that of HP-CZA. Figure 4 illustrates the XRD patterns of CP-CZA and HP-CZA before and after calcination. In Fig. 4(a), the diffraction lines indicate the formation of copper, zinc and aluminium oxide after calcination. The structure of HP-CZA was found to be similar to CP-CZA before as well as after calcination. However, HP-CZA displayed broader peaks compared to CP-CZA, indicating its relatively smaller crystallite size. Based on the Scherrer equation, the crystallite sizes of HP-CZA and CP-CZA after calcination were calculated to be ~7.3 nm and 16.3 nm, respectively. This indicates that homogeneous precipitation method is capable of yielding nano-sized catalyst.

Figure 3 shows SEM images of the HP-derived samples prepared under different reaction conditions and CP-CZA. The sample prepared with 1M urea clearly exhibits a plate-like structure. This morphology further confirms the preferred orientation observed in the X-ray diffraction pattern as shown in

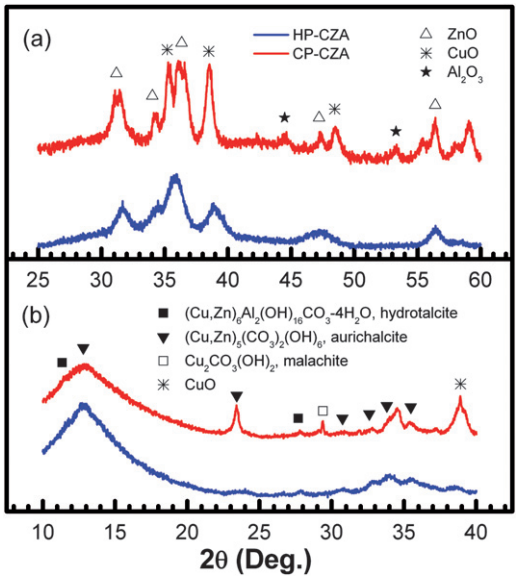

Fig. 4 XRD patterns of CP-CZA and HP-CZA (a) after calcination and (b) precursors.

Fig. 2 (a). When the urea concentration and amount of water were increased, fracturing of surface of the structures was observed, and finally formed the flower-like structures, as shown in Fig. 3(b) and (c). Interestingly, after high temperature calcination (300 °C in air for 3h) and reduction (350 °C in 10% H_2/N_2 for 2h) processes, HP-CZA particles can still maintain the special morphology with scarcely shape reconstruction, even the crystal structure of HP-CZA catalysts is very different from that of precursors, as shown in Fig. 3(e). On the other hand, CP method-derived particles display irregular shape and non-uniform particle size. Both the precursors and the reduced CP-CZA catalysts show serious aggregation, as shown in Fig. 3(d) and (f). From BET analysis, the surface area of calcined HP-CZA and CP-CZA catalysts were calculated to be 78.5 m^2/g and 47.3 m^2/g, respectively. This flower-like morphology of HP-CZA particles is presumably responsible for the larger specific surface area than that of the CP-CZA particles, and is expected to facilitate the methanol reforming reaction.

Measurements of catalytic activity and methanol reforming reaction

The TPR profiles of the catalysts prepared by HP and CP methods are presented in Fig. 5, with pure CuO data as a comparison. In Fig. 5(a), all samples exhibit a reduction profile in the temperature range 100–350 °C. Unlike the curve of pure CuO, both HP and CP catalysts show less H_2 consumption and asymmetric TPR profiles; and the main reduction peaks shift to either higher (CP) or lower (HP) temperature relative to that of CuO. For CP-CZA, the onset of the reduction is apparent at 150 °C and increases rapidly to reach a maximum at 248 °C. Moreover, a shoulder at 280 °C and completion of the reduction at about 320 °C is concluded. In contrast, HP-CZA exhibits a lower onset reduction temperature at 115 °C and reaches a maximum at 179 °C. Also different from CP-CZA, it shows a long tail at 200 °C and extends the reduction process to 265 °C.

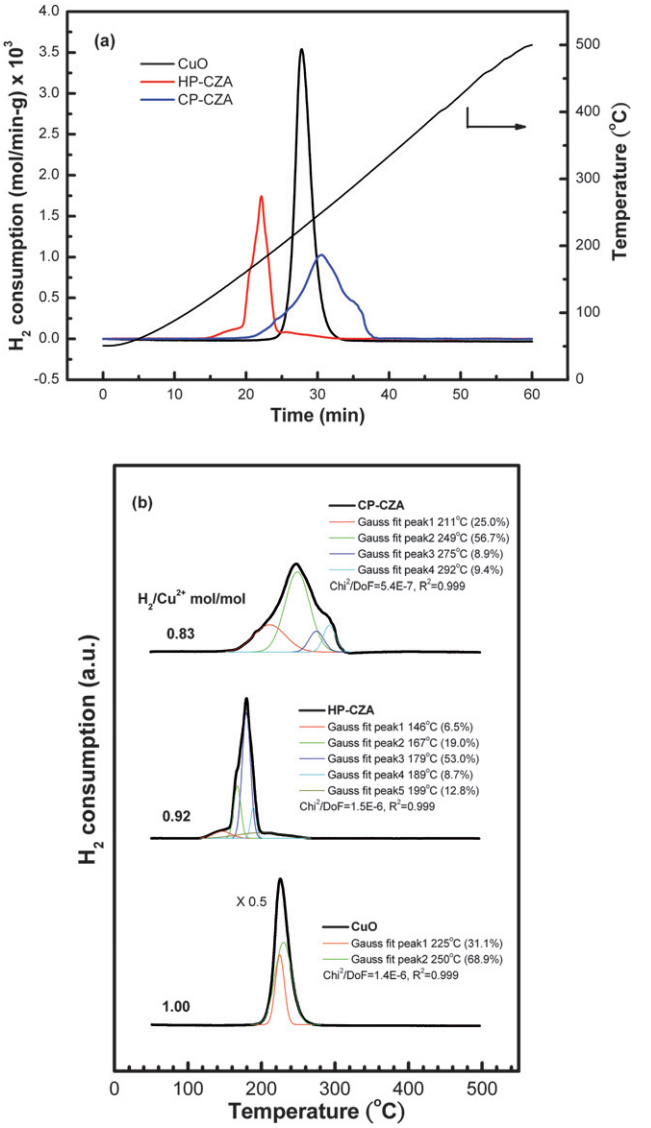

Fig. 5 Temperature Programmed Reduction patterns with Gaussian fitting results and the extent of reduction of CuO, HP-CZA, and CP-CZA.

It is clear that the catalyst prepared by HP method shows a lower reduction temperature and narrower range, indicating better dispersion of copper in the catalyst and easier reduction of the copper oxides in HP-CZA catalyst.

In order to get more insight into the TPR results, the profiles were deconvoluted by fitting to Gaussian profiles as summarized in Fig. 5(b). There are at least four components in the deconvolution, manifesting the complexity of these reduction reactions. Different TPR components were explained by reduction of different Cu(II) species, such as CuO, $CuAl_2O_4$, and Cu^{2+} ions incorporated in octahedral sites of the Al_2O_3 phase.[13,22,29] For the curve of CuO, it can be distinguished into two TPR components which could be interpreted as the two-step reduction: Cu(II) → Cu(I) → Cu(0).[30] Since the XRD results of HP and CP catalysts, shown in Fig. 4(a), illustrate clear CuO diffraction lines, the main peaks in the TPR profiles should also be assigned to the reduction of CuO. Excluding CuO, Cu(II) species in the zinc oxide and zinc aluminate should be reduced at a temperature higher than that of CuO,[29] and could be related to the small signal that appears at the end of the reduction peak. It also has been reported that highly dispersed copper in CZA catalysts would exhibit Cu–Al interaction in the calcined samples.[31] The principal role of aluminium oxide would be to enhance the dispersion of oxidic copper species on its surface, both by the formation of a $CuAl_2O_4$-like phase and by the stabilization of isolated Cu^{2+} ions in the alumina matrix. The reduction of copper in $CuAl_2O_4$-like species located at lower temperatures than CuO.[13] Although we can not observe such phase in the XRD analysis, there is a possibility that small amount of $CuAl_2O_4$-like species would form within the catalyst. This could be the reason for the small TPR components at the beginning of the reduction peak. The shape variation of TPR curves of the HP and CP catalysts could also be attributed to the different specific surface area, crystallite size of copper, and the metal-support interaction.[22]

It is interesting to note that most of the reduction temperatures of HP-CZA are below 200 °C, which are much lower than those of the CP-CZA. Moreover, the reduction temperature range for HP-CZA is 16 °C, which is only about 2/3 of the temperature range for CP-CZA. In Fig. 5(b), HP-CZA shows around 10% enhanced reduction (H_2/Cu^{2+} molar ratio) (0.92) than that of CP-CZA (0.83), which is correlated with the smaller CuO crystallites of HP-CZA than that of CP-CZA as indicated in Fig. 4. The abovementioned observation clearly indicates the improvement in activity and uniformity of the HP-CZA catalyst. From the XRD results in Fig. 4(b), HP-CZA is hydrotalcite-like structure after the precipitation process, while CP-CZA shows obvious CuO and malachite structures besides the hydrotalcite-like phase. These uniform structures in HP-CZA not only affect the distribution of the copper, but also the metal-support interaction, leading to the improved reactivity in HP-CZA, particularly after the calcination treatment.

Table 1 summarizes the results for steam reforming of methanol at 250 °C using the CZA catalysts prepared by both CP and HP methods. The commercial CZA catalyst (G66B) is also used as a comparison. The catalyst prepared by HP method clearly shows higher efficiency for methanol conversion, which can be attributed to the higher surface area and excellent dispersion of active metal in this catalyst. The turnover frequency (TOF) of HP-CZA catalysts is higher than that of CP-CZA and commercial CZA, indicating higher active copper surface of the HP sample. Significant enhancements in the rate of hydrogen production as well as selectivity of carbon dioxide are also observed, suggesting the homogeneous precipitation method to be a superior way to prepare highly active catalyst for the methanol reforming reaction.

Modification of support of the CZA catalysts with cerium and zirconium oxides

The functions of cerium and zirconium oxides in the Cu-based catalyst system over methanol reforming reaction have been extensively studied in the literatures.[9,32–40] CeO_2 has been introduced to increase the Cu dispersion and the thermal stability of the catalysts,[34,35] and even to reduce the CO concentration due to its ability to store/release O_2 by Ce^{4+}/Ce^{3+} redox couple.[36] Moreover, ZrO_2 is also expected to enhance the catalytic behavior of Cu-based catalysts. The higher activity of Cu-ZrO_2

Table 1 Comparison of CP-CZA and HP-CZA over the OMR reaction at 250 °C for 5h

Catalyst	Chemical composition[a] (wt%)			Synthesis pH value	S_{BET} (m^2/g)	S_{Cu} (m^2/g)	Dispersion (%)	Methanol conversion (%)	H_2 production (mmol/sec-Kg_{cat})	TOF[b] (s^{-1})	Selectivity (%)	
	Cu	Zn	Al								CO_2	CO
CP-CZA	43.1	46.2	10.7	7.77	47.3	19.6	7.6	77.0	145.3	0.29	97.2	2.8
HP-CZA	44.7	45.8	9.5	7.63	78.5	24.3	10.2	90.1	198.9	0.33	98.7	1.3
Commercial CZA (G66B)	38	41	21		70.1	21.0	8.1	88.7	157.4	0.30	98.1	1.9

[a] Chemical compositions obtained from ICP measurement. [b] Hydrogen molecules produced per unit surface atom per second at 250 °C.

Table 2 CZACZ catalyst series over the OMR reaction at 250 °C for 5h

Catalyst	Composition					S_{BET} (m^2/g)	S_{Cu} (m^2/g)	Dispersion (%)	Methanol conversion (%)	H_2 (mmol/sec-Kg_{cat})	TOF (s^{-1})	Selectivity (%)	
	Cu	Zn	Al	Ce	Zr							CO_2	CO
CZA	45	45	10			78.5	24.3	10.2	90.1	198.9	0.33	98.7	1.3
CZAC	45	45	5	5		83.6	28.5	11.4	91.5	217.2	0.31	99.1	0.9
CZACZ	45	45	5	2.5	2.5	81.3	29.1	11.8	90.7	213.5	0.30	99.1	0.9
CZC	45	45		10		81.5	29.9	12.5	93.3	238.6	0.32	99.2	0.8
CZCZ	45	45		5	5	82.8	30.7	13.1	95.9	244.1	0.32	99.3	0.7

catalysts has been attributed to the stabilization of Cu_2O on the surface of the reduced catalysts.[9,17,37] It is believed that the formation of Cu_2O leads to both more active and more durable catalysts, since Cu_2O is less susceptible to sintering than Cu metal.[9,37] Therefore, in the present research, cerium and zirconium oxides were incorporated to support CZA catalyst in order to further improve its catalytic properties. The compositions of modified catalysts are listed in Table 2. Since the high activity CZA catalyst has been prepared by homogeneous precipitation in the present study, similar preparation conditions were used to prepare the modified catalysts.

Fig. 6 presents the EDX mapping pattern of CZCZ catalyst. Not only copper and zinc can be seen to be dispersed uniformly in the catalyst, but cerium and zirconium are also distributed quite uniformly between copper, zinc, and each other. This high homogeneity of metal components in the precursor should result from the homogeneous hydrolysis ions in the precursor solution generated *via* HP method. The EDX mapping of CZCZ in Fig. 6 indicates that HP method is able to produce highly dispersed metal components in the catalyst precursor, which plays an important role in the formation of working catalyst after calcination, and may enhance its catalytic performance over the methanol reforming reaction. In addition, it also implies that this method can be used to prepare other multi-compositional materials.

Fig. 7 presents the results of TPR studies of the CZACZ catalyst series. For the catalysts containing alumina, as shown in Fig. 7 (a), (b), and (c), the reduction temperature can be seen to be around 180 °C. However, for the catalysts without alumina as shown in Fig. 7 (d) and (e), the reduction temperature clearly decreases to around 160 °C. The 20 °C lower reduction temperature of main peaks indicates that HP-CZC and HP-CZCZ have higher Cu dispersion, and are likely to exhibit

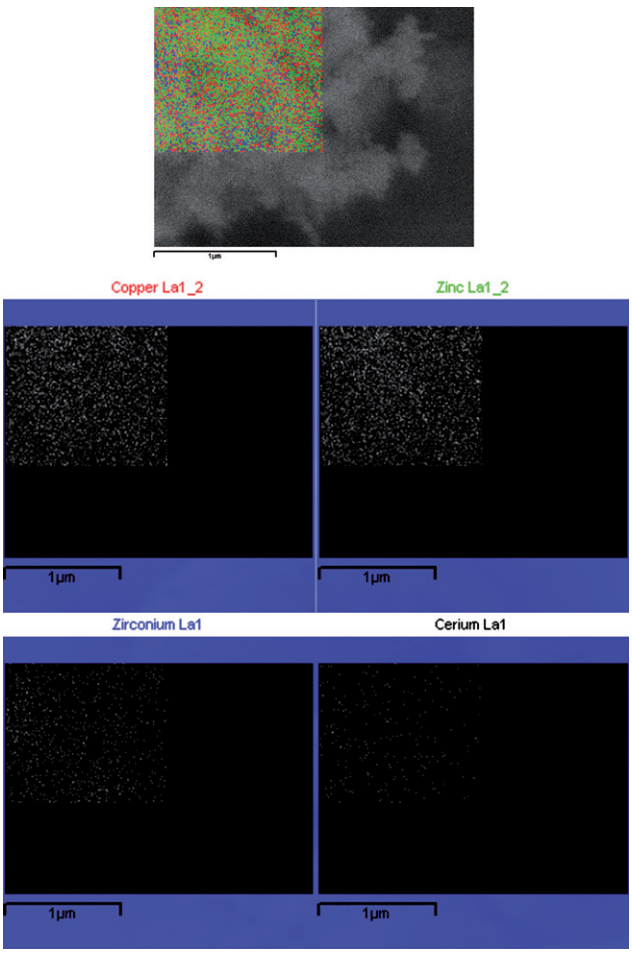

Fig. 6 EDX mapping of HP-CZCZ catalyst.

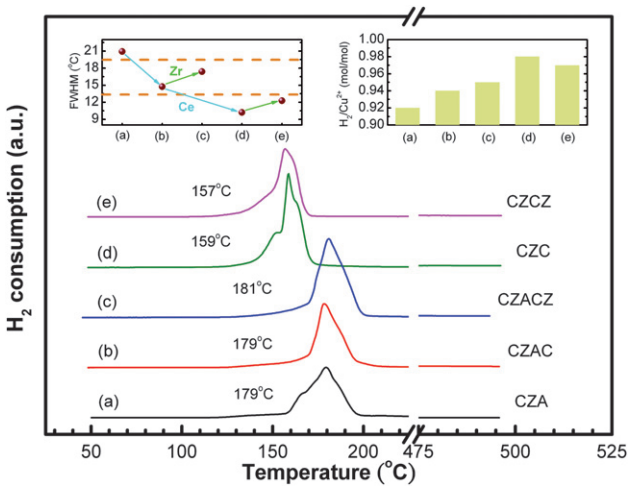

Fig. 7 TPR results of (a) CZA (b) CZAC (c) CZACZ (d) CZC and (e) CZCZ prepared by HP method. The insets illustrate the FWHM of the reduction peaks (left) and the extent of reduction for each sample (right).

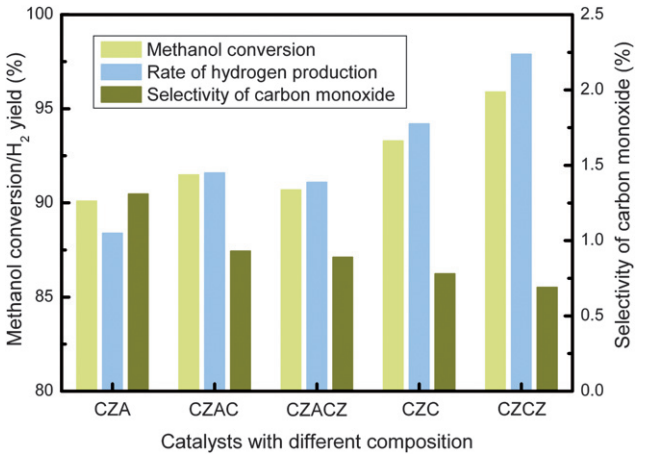

Fig. 8 Oxidative methanol reforming results of HP-CZA modified *via* addition of Ce and Zr oxides.

higher catalytic activity over the reforming reaction than the other catalysts. As shown in Table 2, the measurements of copper surface area and dispersion also have the same trend as TPR results.

The insets in Fig. 7 demonstrate the full width half maximum (FWHM) of the reduction peaks and the extent of reduction (H_2/Cu^{2+} molar ratio) for each samples. In Fig. 7, all the catalysts prepared by HP method exhibit high extent of reductions, especially over 95% for CZC and CZCZ, indicating that these two catalysts have better activity than the others, which also reflects on their low reduction temperatures. Moreover, it is interesting to note that for the catalysts with cerium oxide, the FWHM of the reduction peak decreases dramatically. When there is no alumina in the catalyst, the FWHM is even smaller. On the other hand, for the samples with zirconium oxide, the FWHM of reduction peaks increase slightly whether there is alumina in the catalyst or not. This result manifests that addition of alumina and zirconium oxides can enhance the interaction between copper and the support, resulting in broader TPR profiles. Despite broadening the TPR profiles, alumina and zirconium oxides can act as a diffusion barrier to prevent sintering of copper and cerium oxides during methanol reforming reaction and improve the catalytic stability.[19,38]

The results of methanol reforming reaction at 250 °C for HP-CZACZ catalyst series are illustrated in Fig. 8 and the details of the reaction are summarized in Table 2. For the catalysts containing alumina, the methanol conversion was found to be around 90%. Addition of cerium and zirconium oxides increased the hydrogen production rate and decreased the CO concentration. When alumina are completely substituted by cerium and zirconium oxides, both the methanol conversion as well as hydrogen production rate further increase, while the CO concentration decreases to around 0.7% which is approximately half of the HP-CZA catalyst. Although the TOFs don't have much change after modification of cerium and zirconium oxides, the hydrogen production rates show obvious increase, especially for CZC and CZCZ catalysts. Comparative to the similar catalysts operated at 250 °C over methanol reforming reaction in literature,[38,39] our modified catalysts exhibit nearly 100% methanol conversion and over 200 mmol/sec-Kg_{cat}, at merely 20 mg catalyst loading under high gas feeding rate (GHSV > 8500 h^{-1}), manifesting the advantage of our catalysts.

Modification of this catalyst with cerium not only greatly enhances the methanol conversion and rate of hydrogen production, but it also significantly reduced the formation of CO, which may be due to the high oxygen storage capacity of cerium oxide.[36,40] In our observation, incorporation of zirconium can further improve the catalytic behavior. Besides, addition of cerium and zirconium oxides may facilitate the water–gas shift reaction (Eq. (5)), consequently causing the CO to be oxidized by H_2O, thus resulting in increased production of hydrogen and reduced concentration of CO simultaneously.[36,38] As shown in Fig. 8, for HP-CZCZ catalyst, the hydrogen production rate increases to as high as 98% and the methanol conversion rises to as high as 96% as well. After 100 hour stability test, this catalyst exhibits 0.15% decay of methanol conversion per hour. Although the independent function of CeO_2 and ZrO_2 in the Cu-based catalyst system has been reported,[9,38,39] the joint function of these two oxides as well as the relations among each component in the catalyst are still unclear. We believe this joint function would also affect the catalytic behavior.

Conclusions

Highly active catalysts for hydrogen production were successfully prepared by a homogeneous precipitation method under optimized conditions. The CZA catalysts thus synthesized using the homogeneous precipitation method exhibited highly uniform dispersion of components and significantly lower reduction temperature as compared to the conventional co-precipitation method. In particular, the flower-like morphology of the catalyst particles suggests that the homogeneous precipitation method affords a higher specific surface area. Over the methanol reforming reaction, the catalysts prepared by HP method exhibited greatly improved performance in terms of methanol conversion, yield of hydrogen production, and higher carbon dioxide selectivity than the catalysts prepared by CP method. When the alumina support was substituted by cerium and

zirconium oxides, the reduction temperature was further decreased while simultaneously further improving the catalytic reaction performance. Moreover, merely 20 mg catalyst loading exhibited 98% methanol conversion rate under higher than 8500h^{-1} GHSV, indicating that HP-derived catalyst are capable of producing hydrogen highly efficiently. In future, not only can this method be used to synthesize other multi-composition materials with high homogeneity, but can also be used for large scale production of highly active catalyst that can generate hydrogen efficiently for fuel cell applications.

Acknowledgements

The work is supported by the National Science Council, Academia Sinica, Ministry of Education in Taiwan, and AOARD under Air Force Office of Scientific Research, USA.

References

1 P. Kluger, *Int. J. Hydrogen Energy*, 2001, **26**, 1137–1147.
2 J. M. O. Bockris, *Int. J. Hydrogen Energy*, 1999, **24**, 1–15.
3 W. H. Cheng, *Acc. Chem. Res.*, 1999, **32**, 685–691.
4 I. A. Fisher and A. T. Bell, *J. Catal.*, 1999, **184**, 357–376.
5 M. S. Spencer, *Top. Catal.*, 2003, **22**, 135–135.
6 L. Alejo, R. Lago, M. A. Pena and J. G. L. Fierro, *Appl. Catal., A*, 1997, **162**, 281–297.
7 J. Agrell, K. Hasselbo, K. Jansson, S. G. Jaras and M. Boutonnet, *Appl. Catal., A*, 2001, **211**, 239–250.
8 T. Shishido, Y. Yamamoto, H. Morioka, K. Takaki and K. Takehira, *Appl. Catal., A*, 2004, **263**, 249–253.
9 H. Oguchi, T. Nishiguchi, T. Matsumoto, H. Kanai, K. Utani, Y. Matsumura and S. Imamura, *Appl. Catal., A*, 2005, **281**, 69–73.
10 B. L. Kniep, F. Girgsdies and T. Ressler, *J. Catal.*, 2005, **236**, 34–44.
11 S. Velu, K. Suzuki and T. Osaki, *Chem. Commun.*, 1999, 2341–2342.
12 S. Velu, K. Suzuki, M. P. Kapoor, F. Ohashi and T. Osaki, *Appl. Catal., A*, 2001, **213**, 47–63.
13 S. Murcia-Mascaros, R. M. Navarro, L. Gomez-Sainero, U. Costantino, M. Nocchetti and J. L. G. Fierro, *J. Catal.*, 2001, **198**, 338–347.
14 Y. G. Lin, Y. K. Hsu, S. Y. Chen, Y. K. Lin, L. C. Chen and K. H. Chen, *Angew. Chem., Int. Ed.*, 2009, **48**, 7586–7590.
15 J. Agrell, M. Boutonnet, I. Melian-Cabrera and J. L. G. Fierro, *Appl. Catal., A*, 2003, **253**, 213–223.
16 Y. Kawamura, K. Yamamoto, N. Ogura, T. Katsumata and A. Igarashi, *J. Power Sources*, 2005, **150**, 20–26.
17 J. Agrell, H. Birgersson, M. Boutonnet, I. Melian-Cabrera, R. M. Navarro, S and L. G. Fierro, *J. Catal.*, 2003, **219**, 389–403.
18 A. Mastalir, B. Frank, A. Szizybalski, H. Soerijanto, A. Deshpande, M. Niederberger, R. Schomacker, R. Schlogl and T. Ressler, *J. Catal.*, 2005, **230**, 464–475.
19 P. H. Matter and U. S. Qzkan, *J. Catal.*, 2005, **234**, 463–475.
20 M. Ronning, F. Huber, H. Meland, H. Venvik, D. Chen and A. Holmen, *Catal. Today*, 2005, **100**, 249–254.
21 T. Shishido, Y. Yamamoto, H. Morioka and K. Takehira, *J. Mol. Catal. A: Chem.*, 2007, **268**, 185–194.
22 M. Turco, G. Bagnasco, U. Costantino, F. Marmottini, T. Montanari, G. Ramis and G. Busca, *J. Catal.*, 2004, **228**, 43–55.
23 G. C. Bond and S. N. Namijo, *J. Catal.*, 1989, **118**, 507–510.
24 R. J. Candal, A. E. Regazzoni and M. A. Blesa, *J. Mater. Chem.*, 1992, **2**, 657–661.
25 G. J. A. A. Soler-Illia, R. J. Candal, A. E. Regazzoni and M. A. Blesa, *Chem. Mater.*, 1997, **9**, 184–191.
26 M. H. Marjorie and B. M. Kariuki, *Acta Crystallogr., Sect. B: Struct. Sci.*, 1994, **50**, 673–676.
27 M. Kockrling, G. Geismar, G. Henkel and H. F. Nolting, *J. Chem. Soc., Faraday Trans.*, 1997, **93**, 481–484.
28 J. W. Couves, J. M. Thomas, D. Waller, R. H. Jones, A. J. Dent, G. E. Derbyshire and G. N. Greaves, *Nature*, 1991, **354**, 465–468.
29 S. Velu, K. Suzuki, M. Okazaki, M. P. Kapoor, T. Osaki and F. Ohashi, *J. Catal.*, 2000, **194**, 373–384.
30 B. Linstrom, L. J. Pettersson and P. G. Menon, *Appl. Catal., A*, 2002, **234**, 111–125.
31 R. T. Figueiredo, A. Martinez-Arias, M. Lopez Granadoz and J. L. G. Fierro, *J. Catal.*, 1998, **178**, 146–152.
32 S. Patel and K. K. Pant, *J. Power Sources*, 2006, **159**, 139–143.
33 A. Szizybalski, F. Girgsdies, A. Rabis, Y. Wang, M. Niederberger and T. Ressler, *J. Catal.*, 2005, **194**, 373.
34 Y. Liu, T. Hayakawa, K. Suzuki, S. Hamakawa, T. Tsunoda, T. Ishii and M. KuMagai, *Appl. Catal., A*, 2002, **223**, 137–145.
35 S. Patel and K. K. Pant, *Appl. Catal., A*, 2009, **356**, 189–200.
36 J. Kaspar, P. Fornasiero and M. Graziani, *Catal. Today*, 1999, **50**, 285–298.
37 H. Oguchi, H. Kanai, K. Utani, Y. Matsumura and S. Imamura, *Appl. Catal., A*, 2005, **293**, 64–70.
38 G. Huang, B. J. Liaw, C. J. Jhang and Y. Z. Chen, *Appl. Catal., A*, 2009, **358**, 7–12.
39 S. D. Jones and H. E. Hagelin-Weaver, *Appl. Catal., B*, 2009, **90**, 195–204.
40 P. Fornasiero, R. Di Monte, G. Ranga Rao, J. Kaspar, S. Meriani, A. Trovarelli and M. Graziani, *J. Catal.*, 1995, **151**, 168–177.

